

Charge Density Wave Order in the Topological Insulator Bi_2Se_3

Yanan Li¹, Christian Parsons¹, Sanath Ramakrishna², Anand Dwivedi¹, Marvin Schofield¹, Arneil Reyes², and Prasenjit Guptasarma¹

¹Department of Physics, University of Wisconsin-Milwaukee, Milwaukee, Wisconsin 53211, USA ²National High Magnetic Field Laboratory/Florida State University, Tallahassee, Florida 32310, USA

Abstract

Hexagonally deformed Fermi surfaces and strong nesting, found in topological insulators (TIs) such as Bi_2Se_3 and Bi_2Te_3 over the past decade, have led to several predictions of possible Density Wave order in these systems. Recent evidence for strong Fermi nesting in superconducting $\text{Cu-Bi}_2\text{Se}_3$ and $\text{Nb-Bi}_2\text{Se}_3$ has led to further speculation about the importance of charge order in the context of unconventional superconductivity. Here, we report what we believe is the first direct observation of Charge Density Wave (CDW) order in Bi_2Se_3 . Our results include the observation of a 140K metal-insulator-metal transition in resistivity as a function of temperature. We corroborate this with nuclear magnetic resonance (NMR) studies of the spin-lattice relaxation ($1/T_1$) rate of the ^{209}Bi nucleus, which also displays a transition at 140K. Additionally, we use electron diffraction to reveal a periodic lattice distortion (PLD) in Bi_2Se_3 , together with diffuse charge order between \vec{k} and $\vec{k} \pm \Delta\vec{k}$. This diffuse scattering points toward the presence of an incommensurate charge density wave (I-CDW) above room temperature, which locks into a CDW upon cooling below $\sim 140\text{K}$. We also observe two additional transitions in $1/T_1$ near 200K and 15K. The transition at 200K appears to display some anisotropy with the direction of applied magnetic field. In this report, we focus on the CDW transition at 140K. We include some speculation of the two other transitions observed at 15K and 200K by NMR, also revealed here for the first time.

INTRODUCTION

The 2D layered chalcogenide Bi_2Se_3 and its intercalated versions continue to elicit significant interest due to the presence of non-trivial topological surface states protected by time reversal symmetry, along with fascinating properties of nematic order and superconductivity.¹⁻⁶ Ideally, Bi_2Se_3 is a 3D topological insulator with a single Dirac cone within a substantial bulk energy gap (0.3 eV).⁷ However, several experiments have observed a lowering of the bulk conduction band due to natural electron doping from vacancies or antisite defects crossing the Fermi energy and allowing for bulk electron conduction.⁸⁻¹¹ Under high pressure, or upon intercalating with metals such as Cu and Nb, Bi_2Se_3 displays unconventional superconductivity.¹²⁻¹⁴ Most unconventional superconductivity arises out of strong electron-electron correlations.¹⁵⁻¹⁸ However, Bi_2Se_3 displays weak sp electron correlation.^{19,20} This conundrum has led to a search for other possible mechanisms for unconventional electron pairing in Cu-, Sr- and Nb- intercalated Bi_2Se_3 . An idea that has gained ground in recent years is based on Fermi nesting. First principles calculations on $\text{Cu}_x\text{Bi}_2\text{Se}_3$ ¹ in combination with elastic neutron diffraction measurements on $\text{Sr}_{0.1}\text{Bi}_2\text{Se}_3$ ² indicate that singular electron-phonon interactions with strong Fermi nesting at long wavelength can lead to pseudo-triplet pairing with A_{2u} symmetry. In addition to this, there is now strong evidence that with contributions from the bulk, the cross section of the Dirac cone in Bi_2Se_3 evolves from circular geometry at the Dirac point into a hexagon-like geometry around 350 meV above the Dirac point, and eventually to a hexagram-like geometry near 435 meV above the Dirac point.²¹ The near-flat pieces of such a hexagon in the range $0.55E^* < E < 0.9E^*$ can result in nesting vectors at $Q_i = 2k_{Fe_i}$, $i=1 \dots 3$, where Q_i is the wave vector and k_{Fe_i} is the Fermi momentum.²² Central to a strong Fermi nesting factor is the layered structure of Bi_2Se_3 . Angle-resolved Photoemission Spectroscopy (ARPES) studies on Bi_2Se_3 have confirmed that natural electron-doped Bi_2Se_3 has a hexagonally deformed Fermi Surface. Kuroda et al²¹ have suggested that two flat segments of a hexagonal Fermi surface facing each other across $2\vec{k}_F$ along $\vec{l} - \vec{k}$ could lead to strong nesting. Realistically, this is a deviation from an ideal TI, which has a single Dirac Cone with a circular Fermi surface,²³ and in which the formation of a charge density wave, or a spin density wave, is forbidden. One of the possible outcomes of such Fermi nesting is the appearance of Density Waves. A few studies have hinted at the existence of CDWs in Cu- Bi_2Se_3 ,^{33,34,47} but so far there has been no evidence of a gap opening with temperature variation, indicating a CDW transition. Additionally, there have been no such reports in Bi_2Se_3 . Here, we report for the first time that Bi_2Se_3 undergoes a transition to a CDW state at 140K.

The ground state of a charge density wave (CDW), which is observed mostly in low dimensional materials, is characterized by spontaneously broken translational symmetry. In the simplest case, the 1D Peierls transition can be a first order or a second order transition, characterized by the temperature evolution of the order parameter. In real life, and in more complex systems, the phase transition to a CDW ground state is mostly observed together with commensurate/incommensurate periodic lattice distortions concomitant with the opening of an energy gap at the Fermi level, resulting in a metal-to-insulator like transition in resistivity as a function of temperature. Single crystals with *imperfect chains* (quasi-1D), or *imperfect nestings* (quasi-2D), can lead to such an energy

gap being partially opened. In such situations, a CDW tends to co-occur with a Periodic Lattice Distortion (PLD) such that the PLD and the CDW are commensurate with the periodicity of the underlying atomic lattice distorted by the PLD.⁵² The electronic charge density, which is a scalar quantity and mostly used as an order parameter of a CDW, is coupled with the PLD. In such a situation, the ordered CDW possesses a period that is an integral or a fractional multiple of the period of either the atomic lattice or the PLD. In cases where the CDW periodicity is not represented in the reciprocal lattice by specific vectors \vec{k} , but rather by an entire range of vectors $\vec{k} \pm \Delta\vec{k}$, one observes diffraction patterns with ‘diffuse’ intensity centered around \vec{k} , and often between Bragg reflections, while maintaining the overall symmetry of the underlying lattice. This is a signature of an incommensurate CDW, or I-CDW, which often precedes a CDW transition at lower temperature.^{37-42, 52}

RESULTS

We report here a combination of resistivity, Selected Area Electron Diffraction (SAED) and Nuclear Magnetic Resonance (NMR) studies to reveal that Bi_2Se_3 undergoes a transition to a CDW state at 140K. We observe a 140K metal-insulator-metal transition in resistivity as a function of temperature. Our Nuclear magnetic resonance (NMR) studies of the spin-lattice relaxation ($1/T_1$) rate of the ^{209}Bi nucleus also displays a transition at 140K. Additionally, electron diffraction reveals a periodic lattice distortion (PLD) in Bi_2Se_3 as well as diffuse charge order between \vec{k} and $\vec{k} \pm \Delta\vec{k}$, as described in the previous section. We argue that this diffuse scattering arises from an incommensurate charge density wave (I-CDW) at higher temperature, foreshadowing a transition to CDW order, into which the I-CDW locks upon cooling below $\sim 140\text{K}$. We also identify two other transitions in NMR $1/T_1$ – one near 200K, and another at 15K. The transition near 200K displays an anisotropy with applied magnetic field. We do not yet have clearly identified physical mechanisms for these additional transitions near 200K and 15K, and instead focus on our observation of a CDW transition in Bi_2Se_3 at transition temperature $T_d = 140\text{K}$. We provide some speculations about the 200K and 15K transitions in the discussion section of this paper.

Resistivity measurements

Four-probe DC resistivity measurements, shown in Fig. 1 and Fig. 2, were performed in the 2K-300K temperature range with linearly aligned electrodes on the ab surface of Bi_2Se_3 single crystals, and with the electric field $E \parallel ab$. To ensure reproducibility, we performed measurements on several different pieces of as-grown single crystal. Fig. 1a, b, are results on different pieces from the same batch of as-grown single crystal. Resistivity measurements at zero field all show approximately metallic behavior from room temperature down to around 140 K. Note a sharp upturn in resistivity with decreasing temperature, centered around 140K, followed by a return to metal-like behavior below 140K. In Fig. 1a, with cooling, we see a rise in resistivity from $\sim 1.38 \times 10^{-5} \Omega\text{m}$ to $1.47 \times 10^{-5} \Omega\text{m}$; in Fig. 1b, we observe a rise of $\sim 1.31 \times 10^{-5} \Omega\text{m}$ to $1.36 \times 10^{-5} \Omega\text{m}$, followed in both cases by a return to metal-like behavior at lower temperature. The inset to Fig. 1a,

b show $d\rho/dT$ as a function of temperature, clarifying the inflexion point and onset near 140K. We identify this metal-insulator-metal behavior as resulting from a gap or instability at the Fermi level, correlated with a transition to a CDW ground state.^{24,25}

Heating and cooling cycles performed on the second piece of Bi_2Se_3 shown in Fig. 1b display very weak thermal hysteresis behavior above the onset transition temperature 140K, pointing to the possibility that the 140K transition is an unconventional second order CDW transition.^{26,27} On the other hand, the observation of thermal hysteresis (between heating and cooling) in resistivity above 200K, shown as a solid blue line and a dashed red line in Fig. 1b, points to the presence of a possible first order transition at higher temperature. We believe that this could arise from a transition from normal phase to an incommensurate charge density wave phase at some temperature above room temperature.²⁸ This agrees with our room-temperature electron diffraction data described below, in which we observe the presence of an I-CDW phase. We therefore assign the transition at 140K to a second order transition from I-CDW to CDW. The lack of (or, weak) thermal hysteresis at 140K indicates a possible phonon-mediated unconventional mechanism described further in the discussion section.^{1,2,29,30}

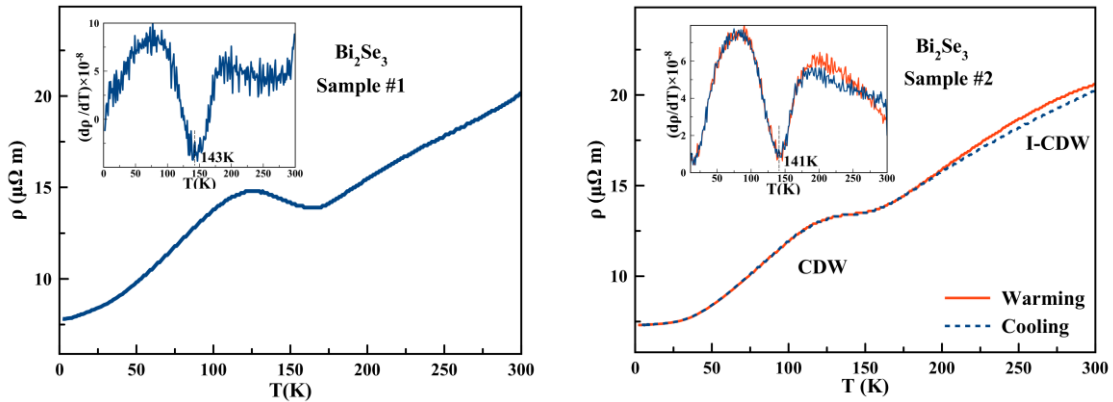


Fig. 1 Resistivity of Bi_2Se_3 as a function of temperature for two different pieces, sample#1 and sample#2, measured in zero magnetic field with the electric field along the ab plane. **a** Measurement on sample #1 while cooling the sample from 300 K to 2 K; **b** Measurement on sample#2 for both cooling and heating. Insets for **a** and **b** are the plots of $d\rho/dT$ as a function of temperature to clarify the temperature values of the inflexion points and the CDW transition temperature T_d .

Fig. 2 examines the magnetic field dependence of T_d for sample#2, same sample as the one shown in Fig. 1b, with magnetic field $H \parallel c$ -axis varying between 0.00T and 4.50T. The inset in Fig. 2 displays $d\rho/dT$ as a function of T , indicating that the transition temperature does not change with applied magnetic field H below 5T. This result is similar to the one obtained for an unconventional CDW in $\text{La}_3\text{Co}_4\text{Sn}_{13}$.²⁶

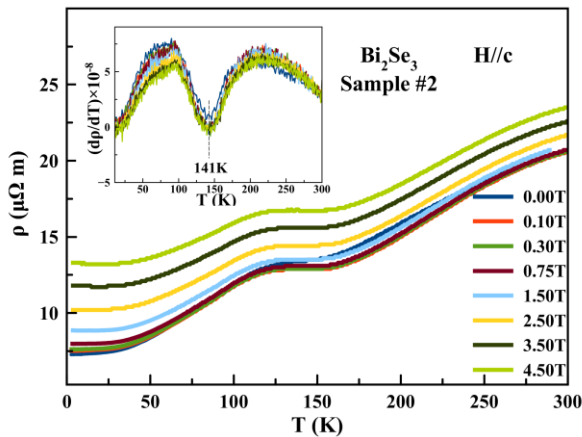


Fig. 2 Thermal dependence of resistivity of Bi_2Se_3 for different values of applied magnetic field H // c -axis varying between 0.00 – 4.50 Tesla.

Electron Diffraction

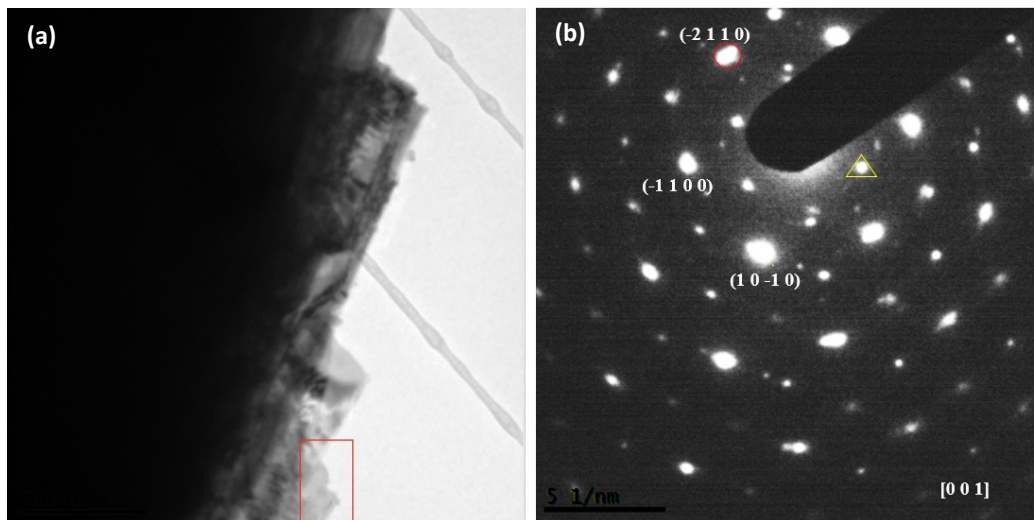


Fig. 3 Transmission Electron Microscopy (TEM) and Selected Area Electron Diffraction (SAED) studies on Bi_2Se_3 single crystal at room temperature. **a** Bright field image of a piece from single crystal of Bi_2Se_3 . The red box indicates the region on which SAED was performed. **b** Electron diffraction along $[001]$ zone axis. Weak reflections of the type identified by a yellow triangle represent normally forbidden reflections from $3a/2$ reflections in the $[001]$ zone axis. Relatively strong reflections, circled in red, are identified reflections from the $[001]$ zone axis.

Fig. 3 and Fig. 4 show Selected Area Electron Diffraction (SAED) performed on Bi_2Se_3 at room temperature. Fig. 3a shows the area from which the diffraction pattern in Figure 3b was obtained along the $[001]$ zone axis. Note, in Fig. 3b, alternate bright and dim spots, with high-intensity spots are identified and circled in red. These features were also observed in SAED by Koski, et al and Wang, et al.^{33,34} Both groups studied the result of intercalation of different zero-valent metals into the van der Waals gaps in Bi_2Se_3 . They

suggest that the most likely reason for the appearance of these weak intensity spots, otherwise forbidden in the cubic-like ABC [001] zone axis in the host Bi_2Se_3 lattice, is the result of a stacking fault. In other words, the presence of zero-valent intercalants in the Van der Waals gap can alter interplanar energetics in such a way as to stabilize hexagonal stacking relative to rhombohedral stacking, resulting in a high density of stacking faults. Based on our XRD results of an increase in c-axis length (shown in supplementary data), and our evidence for stacking faults in SAED, we suggest that the Van der Waals gaps in our Bi_2Se_3 crystals have zero-valent Bi or Se metal resulting from “self-intercalation.” The process of self-intercalation has previously been discussed by several other authors.^{35,36}

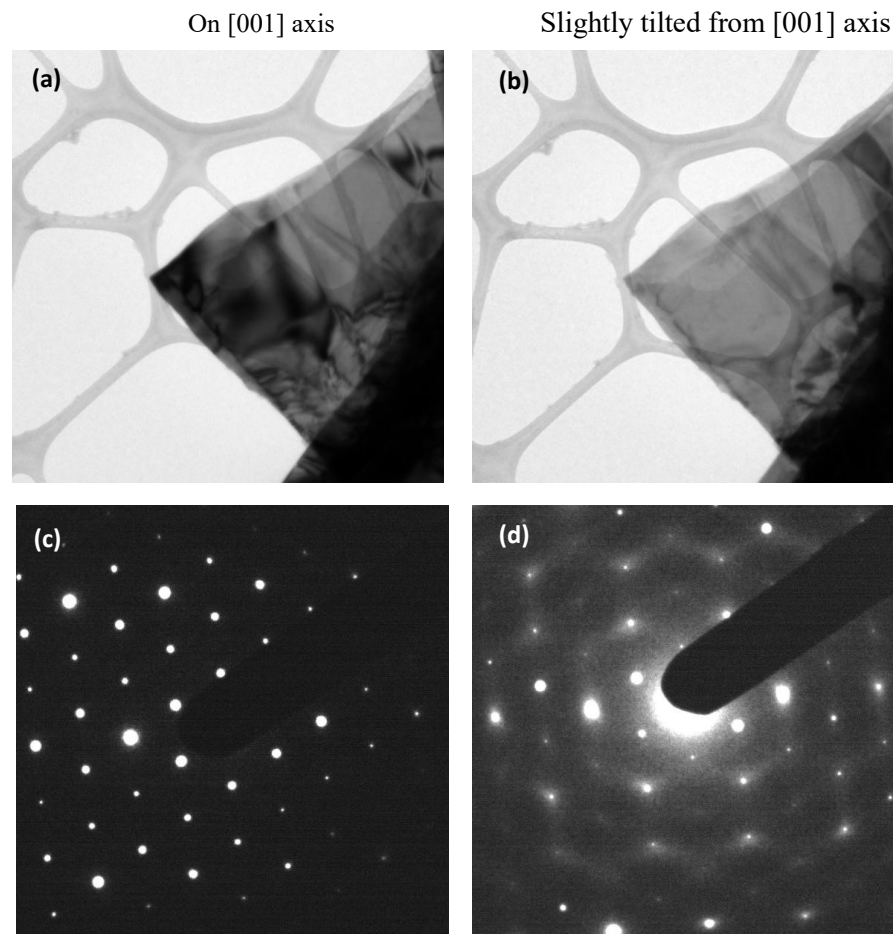
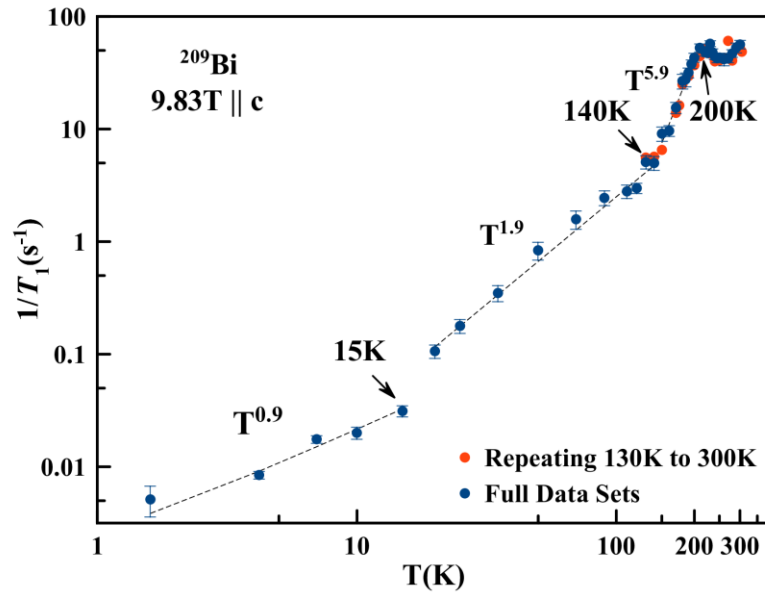


Fig. 4 **a, b** Bright field TEM on a flake obtained from single crystal Bi_2Se_3 . **c, d** Selected Area Electron Diffraction from the corresponding areas shown in (a) and (b). The images in (a) and (c) show results when the beam is on $\langle 001 \rangle$ axis. Images in (b) and (d) show off-axis electron diffraction, for which the sample was tilted slightly (less than 5 degrees) away from zone axis.

Fig. 4 displays bright field TEM and Selected Area Electron Diffraction (SAED) on

flakes obtained from single crystal Bi_2Se_3 . Fig. 4a, c are bright field images on the $\langle 001 \rangle$ zone axis. Fig. 4b, d are taken from the same region of the flake, with the sample tilted slightly (less than 5 degrees) away from the zone axis. The images in Fig. 4c, d correspond to the areas shown in Fig. 4a, b, respectively. As can be seen in Fig. 4d, the diffraction pattern with the crystal tilted slightly off the $\langle 001 \rangle$ zone axis yields diffuse streaks between the diffraction spots. As discussed in previous reports on other similar layered compounds,³⁷⁻⁴² we assign this diffuse intensity as resulting from Periodic Lattice Distortion (PLD) associated with an incommensurate charge density wave (I-CDW), which often occurs as a precursor to a charge density wave (CDW). We have discussed this further in the introduction and discussion sections.

Nuclear Magnetic Resonance



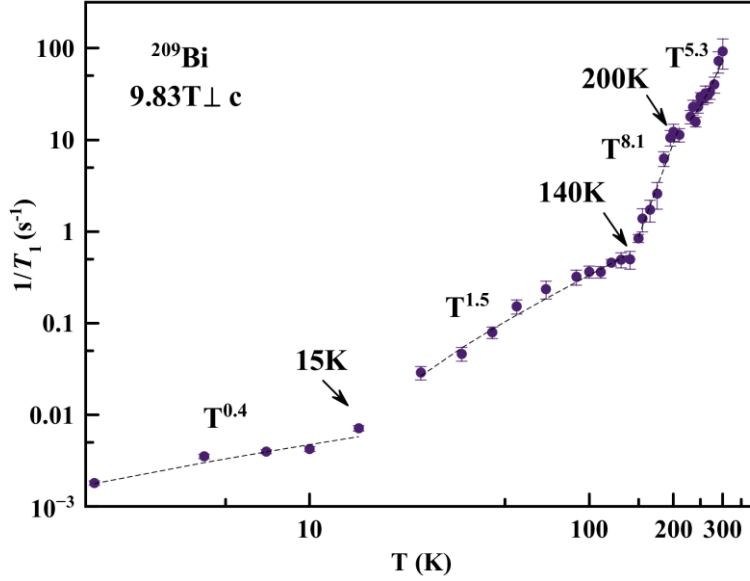


Fig. 5 Spin-lattice relaxation rate ($1/T_1$) shown with temperature T varying between 1.6K and 300K. **a** $H // c$ -axis and **b** $H \perp c$ -axis. Arrows indicate possible transitions at 15K, 140K and 200K. Orange data points shown in (a) represent data obtained from measurements repeated between 130K to 300K in order to confirm the presence of the transition at 200K.

Fig. 5a,b display temperature dependence of the nuclear spin-lattice relaxation rate ($1/T_1$) with varying temperature (1.6K to 300K) with the external magnetic field applied in two orientations, $H//c$ -axis (Fig. 5a) and $H \perp c$ -axis (Fig. 5b) with magnitude of 9.83T. $1/T_1$ measures the recovery of the longitudinal nuclear magnetization following an external perturbation such as an RF field. Following Nissov,⁴³ we applied the standard expression for spin 9/2 nuclei to fit the magnetization recovery $M(t)$, as follows:

$$M(t) = M_0 - 2f \left(\frac{7938}{12155} e^{-45t/T_1} + \frac{1568}{7293} e^{-28t/T_1} + \frac{6}{65} e^{-15t/T_1} + \frac{24}{715} e^{-6t/T_1} + \frac{1}{165} e^{t/T_1} \right),$$

Here, M_0 is the equilibrium magnetization and f is the inversion fraction. The results of this fit are displayed in Fig. 5, where we see three different slope changes: at 15K, 140K, and 200K, labeled with arrows in Fig. 5. We repeated our measurements between 130K and 300K in order to confirm the inflexion observed near 200K. Orange data points indicate these repeat measurements in Fig. 5. The 140K transition coincides with the metal-insulator-metal transition observed in our resistivity measurements. For this reason, we assign the 140K transition to a CDW transition. It is interesting that the 200K transition displays an anisotropy with applied magnetic field. To understand this further, we present Fig. 5, which displays the exponents of T in four different temperature regimes: 0-15K, 15K-140K, 140K-200K, and 200K-300K.

DISCUSSION

The exact nature of Fermi surface distortion, nesting, and density wave instability in a system such as Bi_2Se_3 is critically dependent upon the details of its fermiology. Correlated electron systems typically exhibit intertwined electronic ordered states resulting from degrees of freedom such as lattice, charge, dimensionality, nematicity, and spin – all of which, in turn, tend to be strongly materials-dependent. Thus, many properties of chalcogenides such as Bi_2Se_3 arise from the nature of fluctuations, or overlaps in order parameter, among such intertwined orders. The severity of the overlap tends to be materials-dependent as well. Below, we discuss how materials aspects of Bi_2Se_3 , specifically, can lead to multiple ground states such as that of a charge density wave (CDW). Further, the proximity of superconductivity and density wave orders in many materials begs a discussion of the observed CDW in the context of superconductivity in Bi_2Se_3 , which we think is critical to the understanding of charge order, superconductivity, as well as nematicity.⁴⁴ In this section, we begin with a discussion of the three different transitions found in our measurements. We end by describing important materials considerations which, we believe, drive the multiple (possibly intertwined) order parameters in this layered chalcogenide.

Transition near 140 K:

Nuclear Magnetic Resonance measurements, in Fig. 5a,b, together with resistivity measurements in Fig. 1 and Fig. 2 clearly reveal a transition near 140K. We identify this as a transition to a CDW state below 140K. We support this conclusion from electronic diffraction measurements at room temperature (Fig. 3 and Fig. 4), which reveal the presence of a periodic lattice distortion (PLD), combined with diffuse scattering in off-axis diffraction, suggesting the presence of an incommensurate charge density wave (I-CDW) at room temperature. Interestingly, a careful look at Figure 6, page 075137-4, of Ben-Li Young et al⁴⁵ reveals an anomaly in $1/T_1$ near 140K. Young et al do not mention this transition in their narrative, and do not report results at higher temperature, but we mention this here to confirm that our observations agree with the data in Young et al. To summarize, we believe that Bi_2Se_3 undergoes a transition from an I-CDW to a CDW ground state at 140K, as labeled in Fig. 1b.

Transition near 200K:

Given that the behavior of $1/T_1$ is dependent upon the details of the high temperature phonon spectrum, one would expect it to behave differently above and below the Debye temperature. For Bi_2Se_3 , Debye temperature is $\Theta_D \approx 182\text{K}$. Thus, it is possible that the transition observed around 200K in Fig. 5a,b is due to changes in the phonon spectrum across Θ_D .

Note the anisotropy in this transition with the direction of applied magnetic field, $H//c$ and $H\perp c$, as shown in Fig.5a,b. According to our fits, $1/T_1$ for $H//c$, yields an exponent of $T^{5.9}$ for $140\text{K} < T < 200\text{K}$. It is essentially flat for $200\text{K} < T < 300\text{K}$. For $H\perp c$, $1/T_1$ has a $T^{8.1}$ dependence for $140\text{K} < T < 200\text{K}$ and a $T^{5.3}$ dependence for $200\text{K} < T < 300\text{K}$.

In Fig. 1b, we observe a thermal hysteresis in resistivity above 182K. Whereas a transition across Θ_D would yield a change in slope of resistivity, we are hard-pressed to explain the thermal hysteresis in resistivity, for $T > 182K$, based purely on a Debye temperature transition. A hysteresis between heating and cooling is often observed below a first-order I-CDW to CDW transition. Occasionally, one does not observe a thermal hysteresis, as in the case of 1T-TaS₂.⁵³ In such cases, authors tend to suggest that the transition either is of second order or has some “unconventional” origin.^{29,30,53} In our case, as shown in Fig 1b, the resistivity below 140K does not display a thermal hysteresis. This indicates that the 140K transition is likely a second-order CDW transition. If this reasoning is correct, the 200K transition is a first-order transition.

In the end, we are unsure of the fundamental origin of the transition near 200K. We have identified two possible mechanisms: one based on a 182K Debye temperature transition, and a second based on the nature of the I-CDW. Additional work is needed in order to tease out one mechanism from the other.

Transition near 15K

Fig. 5 also reveals a transition near 15K. This transition agrees with the results in Young et al⁴⁵ for H//c. As shown in Fig.5, our exponents for H//c show the low temperature exponent as $T^{0.9}$ in the range $0 < T < 15K$, and $T^{1.9}$ in the range $15K < T < 140K$. At low temperature, we see a linear Korringa-type relation, $1/T_{1,m} \propto D^2(E_F)T$, where $D^2(E_F)$ is the density of states and $1/T_{1,m}$ includes the magnetic relaxation from conduction electron scattering. This implies that for H //c, the sample behaves like a metal at low temperature. The transition at 15K, in agreement with Young et al, is likely due to a competition between magnetic and quadrupolar scattering.⁴⁵ In the H \perp c case, the low temperature exponent is $T^{0.4}$, corresponding to magnetic relaxation in a semiconductor, for which $1/T_{1,m} \propto NT^{1/2}$, where N is the charge carrier concentration. The difference in low temperature $1/T_1$ power laws in the H//c and H \perp c cases clearly indicates the differences in conduction properties of Bi₂Se₃ along the quintuple layers and across the layers.

The case for a Charge Density Wave in Bi₂Se₃

As discussed earlier, topological insulators such as Bi₂Se₃ and Bi₂Te₃ are expected to host density wave order due to their complex fermiology – in particular, strong Fermi surface nesting.^{21,22} Angle Resolved Photoemission Spectroscopy (ARPES) measurements show that Bi₂Se₃ has a hexagonally deformed Fermi surface. The two parallel segments in the hexagonal Fermi surface separated by $2k_F$ (where, k_F is the Fermi wavevector) can lead to strong nesting and density wave order. Given the topology of the surface states, the two parallel vectors \vec{k} and $-\vec{k}$ could also yield a spin density wave (SDW). However, the Fermi surface is deformed only above 200meV, where bulk bands can become involved. Below 200meV, one finds a pure surface state with a circular constant energy contour.²¹ Thus, bulk states may contribute to Fermi surface deformation, leading to strong Fermi nesting. Shubnikov-de Haas measurements on Nb-Bi₂Se₃ have revealed evidence for a small extra Fermi pocket besides the main Fermi surface of Bi₂Se₃.³ Additionally, a first-principles linear response calculation for Cu-Bi₂Se₃ has revealed a ‘prism-like’ fermi pocket at the Γ point, with opportunities for strong Fermi nesting.¹ Thus, theoretically speaking, the CDW transition reported here is not a surprising result.

When intercalated with Nb, Cu, or Sr, and when subjected to high pressure, Bi_2Se_3 becomes a superconductor with unconventional pairing.^{2,12-14} Strong electron correlations are often found in the vicinity of superconductivity^{17,18} – however *sp* electrons in Bi_2Se_3 are weakly correlated. Xiangang and Sergey¹ suggest that unconventional superconductivity in intercalated layered systems such as $\text{Cu-Bi}_2\text{Se}_3$ might arise from an enhancement of electron-phonon coupling due to strong nesting at long wavelengths. At a certain wave vector q_0 , all pairing channels become degenerate and compete with each other. This singular electron phonon interaction with strong Fermi nesting at long wavelength can provide a large effective coupling constant favoring pseudo-triplet pairing of A_{2u} symmetry in intercalated Bi_2Se_3 .¹ Thus, an interplay of strong spin-orbit coupling, unbroken time-reversal symmetry, and inversion symmetries with certain lattice distortions could lead to enhanced electron-phonon correlations and exotic superconducting states.

As described by Zhu et al⁴⁶, the origin of CDW is strongly related to dimensionality. They describe “Type-I” CDWs as quasi-1D systems with origins in traditional Peierls’ instability and Fermi Surface Nesting (FSN), with lattice distortion being a consequence of the electronic disturbance, as found in linear-chain compounds. Zhu et al assert that “Type-II” CDWs, in contrast, are driven by electron-phonon coupling (EPC) and not by FSN. In such case, the electronic and lattice instabilities are intimately tied to each other with a phonon mode at q_{CDW} which goes to zero at the transition temperature T_d . This second type does not require a metal-insulator transition associated with T_d . They further describe a “Type-III” case, where a charge modulation is found without the driving force of an FSN or EPC, and where the driving force is possibility electron correlations.

Most CDW occurs in quasi-1D or quasi-2D; our current understanding of CDW does not include all the complexities involved in the 3D case, where electron correlations are thought play a primary role.⁴⁶ In this context, it is instructive to further discuss the possible effect of intercalation on k_F anisotropy between k_z versus k_x, k_y . Xiangang and Sergey¹ suggest that small changes in the position of Bi in the *z*-direction can modify the nesting vector $X(q)=\sum\delta(\varepsilon_k)\delta(\varepsilon_{k+q})$, where, ε_k and ε_{k+q} are the energy of states at/near the Fermi level. This nesting vector is largest for wavevector q along the Γ_z direction, when q is close to zero. This can lead to strong Fermi nesting, and strong electron-phonon coupling. Displacement along [001] at small qs (i.e., small momenta) breaks spatial inversion symmetry, lifts double degeneracy, and leads to a large electron-phonon coupling matrix element along this direction close to zone center. Further calculations by Wan, X. & Savrasov, S. Y.¹ and neutron scattering experiments by J. Wang, et al² show broad phonon linewidths for small qs , which could dominate electron-phonon coupling. Based on these arguments, we tentatively pose the possibility of the presence of a quasi-1D Peierls-type transition in the *z*-direction of Bi_2Se_3 .

Electron Diffraction

Room temperature selected area electron diffraction in Figures 2b, 3c, and 3d, taken along the $\langle 001 \rangle$ zone axis, displays the hexagonal symmetry that Bi_2Se_3 is known for.

This is indicated by labeled diffraction spots. Figures 2a, 3a, 3b are bright field Transmission Electron Microscopy images showing the portions of the single crystal where the convergent electron beam was placed. Note the image in Fig. 3d, for images tilted slightly from zone axis. This clearly shows diffuse stripes between diffraction spots. As also discussed in the introduction section of this paper, such diffuse scattering arises from incommensurate lattice distortion concomitant with an incommensurate charge density wave (I-CDW). We use this information, together with our observation of the opening up of a gap near 140K in two bulk measurements (resistivity and NMR T_1) as evidence for a CDW transition at 140K.

Materials considerations

The somewhat elusive nature of superconductivity in single crystals of Cu-Bi₂Se₃, especially the variability of superconducting fraction and T_c to quenching temperature^{47,48}, is likely due to the high sensitivity of electron interactions to actual conditions of quenching and growth. The crystals discussed here were grown using a standard self-flux method, and a higher quenching temperature. The ideal topological insulator, Bi₂Se₃, has separate bulk and surface states. However, experimentally, intrinsic defects and disorder can be widely found in Bi₂Se₃ and intercalated/electron-doped Bi₂Se₃.^{9, 21, 54, 55} Schneeloch et al⁴⁸ used different growth conditions to grow Cu doped Bi₂Se₃ SC and reported that higher temperature quenching (above 560 °C) is essential for superconductivity, especially superconductivity with high diamagnetic shielding fraction. Other growth conditions either cause no SC or weak diamagnetic shielding fraction. This is also our observation⁴⁷ in Cu-Bi₂Se₃. Schneeloch et al suggest that the quenching process either helps maintain a primary intercalated phase or a secondary phase responsible for superconductivity. Huang et al show that high annealing temperature (~600 °C) can cause intercalation of Bi₂ in Bi₂Se₃.³⁵ Our results indicate that higher-temperature quenching leads to strong electron and lattice order, and to interesting electronic ground states such as a CDW or superconductivity.

X-ray diffraction (XRD), shown in supplementary data, reveals that the a-axis value of our Bi₂Se₃ agrees with those of most other reports, but that the c-axis, at 28.66 Å, is 0.02 Å higher than the 28.64 Å reported in most previous reports Bi₂Se₃.^{35,49,50} Huang et al assert that a longer c-axis arises from unintentionally doped Bi-rich flux growth of Bi₂Se₃ where Bi forms a neutral metal Bi₂ layer intercalated into the van der Waals gap.³⁵ They also show that crystals with patches of intercalated Bi show high c-axis values of up to 28.65 Å, close to the c-axis value of 28.66 Å obtained from our Rietveld refinement. XRD results on our Bi₂Se₃ single crystals show no signs of the formation of metastable phases of staged (Bi₂)_m(Bi₂Se₃)_n. The solidification temperature of Bi₂Se₃ (705 °C) is higher than the melting point of both pure Bi (271.4 °C) and pure Se (220 °C). Additionally, Se is a vapor above 685 °C, which is below the solidification temperature of Bi₂Se₃. Consequently, the stoichiometry of Bi₂Se₃ forming at the liquid-vapor interface can be highly dependent upon the vapor pressure of Se at 705 °C. For high annealing temperature (around 600 °C), partial decomposition might occur. Huang presumes that this is due to a large number of Se vacancies created in an evacuated environment,

resulting in liquid Bi in the flux ending up in the van der Waals gaps rather than incorporating into a Bi-Se quintuple layer containing Se vacancies. Our crystals, quenched at higher temperature could lead to Se vacancies and intercalated Bi.

We surmise that, as there is not enough excess Bi to form the metastable phase of staged $(\text{Bi}_2)_m(\text{Bi}_2\text{Se}_3)_n$, excess Bismuth in our crystals forms randomly distributed Bi_2 interlayers in the crystal. The resulting Bi-chains could help form a quasi-1D Peierls-type transition or a quasi-2D type CDW.^{35,46,51} In summary, specific growth conditions are critical to the observation of a CDW or superconductivity in Bi_2Se_3 .

To conclude, we present evidence for the first experimental observation of charge density wave (CDW) order in Bi_2Se_3 . Diffuse streaks in SAED measurements indicate the presence of an incommensurate periodic lattice distortion at room temperature together with diffuse streaks reminiscent of an incommensurate charge density wave (I-CDW). A metal to insulator transition at 140K in resistivity measurements indicates the opening of a CDW-like energy gap. NMR $1/T_1$ measurements further confirms this 140K transition. Using this, together with thermal hysteresis studies of resistivity, we conclude that Bi_2Se_3 displays an unconventional second-order CDW transition temperature at 140K. NMR also reveals two other transitions – one near 15K, and another near 200K. Based on temperature exponents of $1/T_1$, we suggest that the 15K transition results from a competition between magnetic and quadrupolar scattering. The 200K transition is not as clear – we discuss the possibility that this could be sensing a transition across the Debye temperature Θ_D in Bi_2Se_3 , or a transition to a first-order incommensurate CDW. We also discuss how our growth methods promote the formation of a CDW. We suggest that strongly correlated ground states are present in Bi_2Se_3 crystals grown with a high annealing and quenching temperature. In this scenario, the higher temperature growth condition results in self-intercalation of Bi into Bi_2Se_3 , producing in turn a Charge Density Wave transition. Thus, our results suggest a strong dependence of electronic correlations on growth conditions and to the occurrence of ground states such as CDW and superconductivity.

METHODS

Powder X-ray diffraction data were collected from pieces of single crystals powdered inside an inert glove box. Rietveld refinement was performed using GSAS (General Structure Analysis System) and the EXPGUI interface. Selected Area Electron Diffraction (SAED) was performed at room temperature with a Hitachi H-9000NAR high resolution transmission electron microscope (HRTEM) operated at 300 kV. 4-probe resistivity measurements were performed with varying temperature and magnetic field using a Quantum Design Physical Property Measurement System (PPMS).

Pulsed ^{209}Bi NMR (Nuclear Magnetic Resonance) measurements were performed on a Bi_2Se_3 single crystal of crystal size $\sim 0.94 \times 0.58 \times 0.41$ cm placed inside a home-built spectrometer in an 11-Tesla Oxford Helium cryostat. The single crystal of Bi_2Se_3 was

studied with magnetic field oriented in two directions, H//c and H//a. Spin-echo signals for ^{209}Bi NMR spectra were processed using the summed Fourier transform method, with field swept from 9.7T to 10.5T. Spin Lattice relaxation time T_1 measurements in both H//C and H//C directions were performed at stabilized temperature points varying between 1.6K and 300K, with saturation pulses and typical time delays of 10 μs .

REFERENCES

- [1] Wan, X. & Savrasov, S. Turning a band insulator into an exotic superconductor. *Nat Commun* **5**, 4144 (2014).
- [2] Wang, J. *et al.* Evidence for singular-phonon-induced nematic superconductivity in a topological superconductor candidate $\text{Sr}_{0.1}\text{Bi}_2\text{Se}_3$. *Nat Commun* **10**, 2802 (2019).
- [3] Lawson, B. J. *et al.* Multiple Fermi surfaces in superconducting Nb-doped Bi_2Se_3 . *Phys. Rev. B* **94**, 041114(R) (2016).
- [4] Hecker, M. & Schmalian, J. Vestigial nematic order and superconductivity in the doped topological insulator $\text{Cu}_x\text{Bi}_2\text{Se}_3$. *npj Quant Mater* **3**, 26 (2018).
- [5] Matano, K. *et al.* Spin-rotation symmetry breaking in the superconducting state of $\text{Cu}_x\text{Bi}_2\text{Se}_3$. *Nature Phys* **12**, 852–854 (2016).
- [6] Shen, J. *et al.* Nematic topological superconducting phase in Nb-doped Bi_2Se_3 . *npj Quant Mater* **2**, 59 (2017).
- [7] Xia, Y. *et al.* Observation of a large-gap topological-insulator class with a single Dirac cone on the surface. *Nature Phys* **5**, 398–402 (2009).
- [8] Hsieh, D. *et al.* A tunable topological insulator in the spin helical Dirac transport regime. *Nature* **460**, 1101–1105 (2009).
- [9] Hor, Y. S. *et al.* p-type Bi_2Se_3 for topological insulator and low-temperature thermoelectric applications. *Phys. Rev. B* **79**, 195208 (2009)
- [10] Tumelero M. A., Faccio R. & Pasa A. A. The role of interstitial native defects in the topological insulator Bi_2Se_3 . *Physics: Condensed Matter* **28**, 425801 (2016).
- [11] Lahoud, E. *et al.* Evolution of the Fermi surface of a doped topological insulator with carrier concentration. *Phys. Rev. B* **88**, 195107 (2013)
- [12] Kirshenbaum, K. *et al.* Pressure-Induced Unconventional Superconducting Phase in the Topological Insulator Bi_2Se_3 . *Phys. Rev. Lett.* **111**, 087001 (2013).
- [13] Sasaki, S. *et al.* Topological Superconductivity in $\text{Cu}_x\text{Bi}_2\text{Se}_3$. *Phys. Rev. Lett.* **107**, 217001 (2011)
- [14] Asaba, T. *et al.* Rotational Symmetry Breaking in a Trigonal Superconductor Nb-doped Bi_2Se_3 . *Phys. Rev. X* **7**, 011009 (2017)
- [15] Kohama, Y. *et al.* Possible Unconventional Superconductivity in Iron-Based Layered Compound LaFePO : Study of Heat Capacity. *J. Phys. Soc. Jpn.* **77**, 094715 (2008)
- [16] Kiss, T. *et al.* Photoemission Spectroscopic Evidence of Gap Anisotropy in an f-Electron Superconductor. *Phys. Rev. Lett.* **94**, 057001
- [17] Stewart, G. R. Unconventional superconductivity. *Advances in Physics*, **66**, 75-196 (2017)
- [18] Davis, J. C. S. & Lee, D.-H. Concepts relating magnetic interactions, intertwined electronic orders, and strongly correlated superconductivity. *Proc. Natl Acad. Sci.*

- USA* **110**, 17623–17630 (2013)
- [19] Biswas, D., Thakur, S., Balakrishnan, G. & Maiti, K. Exceptional surface and bulk electronic structures in a topological insulator, Bi_2Se_3 . *Sci Rep* **5**, 17351 (2015).
- [20] Hor, Y. S. et al. Superconductivity in $\text{Cu}_x\text{Bi}_2\text{Se}_3$ and its implications for pairing in the undoped topological insulator. *Phys. Rev. Lett.* **104**, 057001 (2010).
- [21] Kuroda, K. et al. Hexagonally Deformed Fermi Surface of the 3D Topological Insulator Bi_2Se_3 . *Phys. Rev. Lett.* **105**, 076802 (2010).
- [22] Fu, L. Hexagonal Warping Effects in the Surface States of the Topological Insulator Bi_2Te_3 . *Phys. Rev. Lett.* **103**, 266801 (2009).
- [23] Zhang, H., Liu, C.-X., & Zhang, S.-C. Spin-Orbital Texture in Topological Insulators. *Phys. Rev. Lett.* **113**, 066801 (2013).
- [24] Duvjir, G. et al. Emergence of a Metal–Insulator Transition and High-Temperature Charge-Density Waves in VSe_2 at the Monolayer Limit. *Nano Letters* **18** (9), 5432–5438 (2018)
- [25] Craven, R. A. & Meyer, S. F., Specific heat and resistivity near the charge-density-wave phase transitions in 2H-TaSe_2 and 2H-TaS_2 . *Phys. Rev. B* **16**, 4583 (1977)
- [26] Welsch, J. et al. Second-order charge-density-wave transition in single crystals of $\text{La}_3\text{Co}_4\text{Sn}_{13}$. *Phys. Rev. Materials* **3**, 125003 (2019)
- [27] Kuo, Y.-K., Lue, C. S., Hsu, F. H., Li, H. H. & Yang, H. D. Thermal properties of $\text{Lu}_5\text{Ir}_4\text{Si}_{10}$ near the charge-density-wave transition. *Phys. Rev. B* **64**, 125124 (2001)
- [28] Zong, A. et al. Ultrafast manipulation of mirror domain walls in a charge density wave. *Sci. Adv.* **4**, 5501 (2018).
- [29] Wezel, J. V., Nahai-Williamson, P., and Saxena S.S. Exciton-phonon-driven charge density wave in TiSe_2 . *Phys. Rev. B* **81**, 165109 (2010).
- [30] Sugawara, K. et al. Unconventional charge-density-wave transition in monolayer 1T-TiSe_2 . *ACS Nano* **10**, 1341 (2015).
- [33] Koski, K. J. et al. Chemical intercalation of zerovalent metals into 2D layered Bi_2Se_3 nanoribbons. *JACS* **134**, 13773–13779 (2012).
- [34] Wang, M. & Koski, K. J. Polytypic phase transitions in metal intercalated Bi_2Se_3 . *J. Phys. Condens. Matter* **28**, 494002 (2016).
- [35] Huang, F.-T. et al. Nonstoichiometric doping and Bi antisite defect in single crystal Bi_2Se_3 . *Phys. Rev. B* **86**, 081104(R) (2012).
- [36] Dai, J. et al. Toward the Intrinsic Limit of the Topological Insulator Bi_2Se_3 . *Phys. Rev. Lett.* **117**, 106401(2016)
- [37] Wilson, J. A., Di Salvo, F. J. & Mahajan, S. Charge-density waves and superlattices in metallic layered transition-metal dichalcogenides. *Adv. Phys.* **24** 117–201(1975)
- [38] Wilson, J. A., Di Salvo, F. J. & Mahajan, S. Charge-density waves in metallic, layered, transition-metal dichalcogenides. *Phys. Rev. Lett.* **32** 882 (1974)
- [39] Williams, P. M., Scruby, C., Clark, W. & Parry, G. Charge density waves in the layered transition metal dichalcogenides. *J. Phys. Colloques.* **37** C4-139–150(1976)
- [40] McMillan, W. L. Landau theory of charge-density waves in transition-metal dichalcogenides. *Phys. Rev. B* **12** 1187 (1975)
- [41] Di Salvo, F. J. & Maurice Rice, T. Charge-density waves in transition-metal compounds *Phys. Today* **32** 32 (1979)
- [42] Li, Y., Smith, N. P., Rexhausen, W., Schofield, M. A. & Guptasarma, P. Possible

- lattice and charge order in $\text{Cu}_x\text{Bi}_2\text{Te}_2\text{Se}$. *J. Phys. Mater.* **3** 015008 (2020)
- [43] Nisson, D. M. et al. Nuclear magnetic resonance as a probe of electronic states of Bi_2Se_3 . *Phys. Rev. B* **87**, 195202 (2013)
- [44] Séamus Davis, J. C. & Lee, D.-H. Concepts relating magnetic interactions, intertwined electronic orders, and strongly correlated superconductivity. *PNAS*. **110**,17623-17630 (2013)
- [45] Young, B.-L. et al. Probing The Bulk Electronic States of Bi_2Se_3 Using Nuclear Magnetic Resonance. *Phys. Rev. B* **86**, 075137 (2012)
- [46] Zhu, X., Cao, Y., Zhang, J., Plummer, E. W. & Guo, J. Classification of charge density waves based on their nature. *Proc. Natl Acad. Sci. USA* **112**, 2367–2371 (2015).
- [47] Smith, Nathaniel P., "Crystal Growth and Manipulation of Intercalated Chalcogenides as Superconductors and Topological Insulators" PhD Thesis, University of Wisconsin Milwaukee (2018).
- [48] Schneeloch, J. A., Zhong, R. D., Xu, Z. J., Gu, G. D., and Tranquada, J. M., Dependence of superconductivity in $\text{Cu}_x\text{Bi}_2\text{Se}_3$ on quenching conditions. *Phys. Rev. B* **91**, 144506 (2015)
- [49] Chiatti, O. *et al.* 2D layered transport properties from topological insulator Bi_2Se_3 single crystals and micro flakes. *Sci Rep* **6**, 27483 (2016).
- [50] Martinez, G. et al. Determination of the energy band gap of Bi_2Se_3 . *Sci Rep* **7**, 6891 (2017).
- [51] Zhu, X., Guo, J., Zhang, J., Plummer, E.W., Misconceptions associated with the origin of charge density waves. *Advances in Physics: X*, **2**, 622-640 (2017)
- [52] Rossnagel, K. On the origin of charge-density wave in select layered transition-metal dichalcogenides. *J. Phys: Condens. Matter* **23** (2011)
- [53] Sugawara, K. *et al.* Unconventional charge-density-wave transition in monolayer 1T-TiSe₂. *ACS Nano* **10**, 1341–1345 (2016).
- [54] Xu, Y., Chiu, J., Miao, L. *et al.* Disorder enabled band structure engineering of a topological insulator surface. *Nat Commun* **8**, 14081 (2017).
- [55] Dai, J. Toward the Intrinsic Limit of the Topological Insulator Bi_2Se_3 . *Phys. Rev. Lett.* **117**, 106401 (2016).